JOURNAL OF MATERIALS SCIENCE **38** (2003) 4541–4549

Reflection from natural fibres: Determination of the scale angle profile

P. VASSIS, E. C. BUTCHER, A. R. LEE
Department of Physics, La Trobe University, Bundoora Victoria 3083, Australia
E-mail: p.vassis@latrobe.edu.au

L. A. HOLT*
Department of Agricultural Sciences, La Trobe University, Bundoora Victoria 3083, Australia

Light of wavelength 632.8 nm scattered from a single natural fibre onto an observation plane perpendicular to the fibre axis was observed to form rings which converge to a point defined by the incident beam. Using a series cone model for natural fibres, these rings are shown to be due to reflection from a curved surface inclined at some angle to the fibre axis, such as scales found on the fibre surface. Measurements of relative intensity and position associated with prominent rings in this observation plane were made. These measurements were used to determine all possible scale angles illuminated by the incident laser beam. Results show that although some 300 scales were illuminated only a few intensity peaks corresponding to prominent rings were detected. Therefore, suggesting that a few prominent scales occur repeatedly within the illuminated section on the fibre. Results also show that both positive and negative scale angles exist along a single fibre. Ranges of scale angles obtained for coarse, fine and super fine wool, mohair and cashmere fibres were found to be: 0.2° to $8.6^\circ \pm 0.05^\circ$, 0.5° to $7.6^\circ \pm 0.05^\circ$, 2.2° to $3.0^\circ \pm 0.05^\circ$, 0.1° to $3.6^\circ \pm 0.05^\circ$, 0.1° to $2.6^\circ \pm 0.05^\circ$ and respectively.

1. Introduction

Appearance of lustre, a desirable attribute of natural fibres, plays an important role in the assessment of fibres, whether it is for textile applications or the evaluation of the health of animal hair, in particular human hair and its care. This assessment however is subjective, and as a result, lustre is not a clearly defined physical parameter that can be easily measured. Lustre is a quality that appears to defy complete measurement. Attempts have been made to quantify it [1–4]. In the determination of lustre, the scattering of light from an array of fibres is measured for oblique incidence and intensity or goniophotometric (GP) curves obtained. It is from these curves that lustre is determined. Single fibres are also used with similar results [5–7]. Lustre of natural fibres is largely associated with surface scale structure of the fibre.

Measurements of scale angle of fibres have generally been determined using two methods. Both methods give only an average value of the scale angle due to the randomness of scale angle in natural fibres and the many scale angles that exist along a single strand of fibre. The first method [3] requires the actual measurement of a sample of scale height and scale length from images of the actual fibre then calculating the scale angle using

$$\text{scale height} = \text{scale length} \tan(\text{scale angle}) \quad (1)$$

The second method [1, 8] calculates the scale angle from goniophotometric (GP) curves. This method requires the measurement of the intensity of scattered light in the plane of the fibre for both orientations of the fibre. Typically, several fibres are aligned parallel to each other with the same fibre orientation. An analogue detector is used and the measurements are taken from a position along the fibre axis to the position perpendicular to the fibre axis. From the intensity measurements, two broad peaks are observed similar to those shown in Fig. 1. Each peak on the GP curve is displaced by an angle of $\pm 2 \times$ (scale angle) [1] from the expected angle of reflection from the fibre axis or the angle between these peaks $4 \times$ (scale angle) [8]. The peaks are thought to be largely attributable to direct specular reflection from the air-cuticle interface of the scale. The scale angle of the fibre is thus determined from the displacement of the peaks from the expected angle of reflection if the fibre had no scales.

This method only gives one value for the scale angle of the fibre, the value indicated by the main peak observed which is attributed to the average scale angle. This, however, is not the case as it is a measure of the scale angle, which corresponds to the scale yielding the strongest reflected intensity, and the very broad nature of the peak suggests that specular reflection from scales with different scale angles occur. Therefore, the

*Presently at UV Eclipse Pty Ltd.

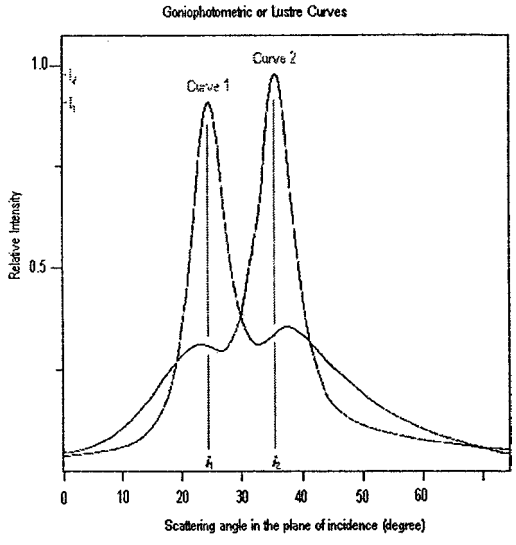

Figure 1 Typical goniophotometric or lustre curves taken for a group of 21 hair fibres, separated by 0.423 mm. Curve 1 and curve 2 are the curves for the same fibre but with opposite orientations, that is the fibre root ends right and left respectively. The angle of incidence i is 30°. From the curves the scale angle ε is calculated by $2\varepsilon = |i - i_1|$ or $2\varepsilon = |i - i_2|$ as determined by Stamm; or $4\varepsilon = i_2 - i_1$ as determined by Fourt.

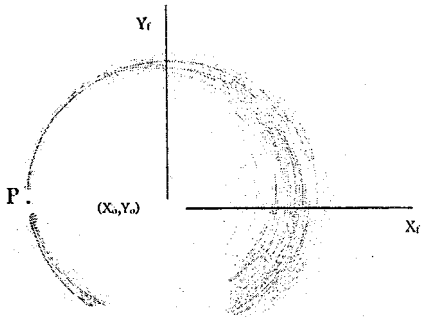

Figure 2 A positive image of light scattered from a Cr coated wool fibre at an angle of incidence of 70° and a beam wavelength of 632.8 nm obtained by rear projection. This image was sharpened to show the rings of primary interest, that is, the rings which meet at point P.

scale angle recorded is just one value in a group of several values.

In this paper, light scattered from a natural fibre is discussed and a method is proposed that will enable all scale angles illuminated by a laser beam to be calculated. This method uses the scattering pattern shown in Fig. 2, obtained by rear-projection of the light reflected from a fibre illuminated at oblique incidence. The scattering pattern shows a group of rings which converge at the point P, the point defined by the incident beam. This group of ring is used to determine the scale angle by taking an intensity profile along the line Y_oY_f.

2. Experimental procedure

In this experiment, a fibre was irradiated with a monochromatic light beam at an oblique angle of incidence, where the fibre and the incident laser beam lie in the same plane. The reflected light was then captured on a screen perpendicular to the fibre axis as shown in Fig. 3. The resulting image was then recorded using photographic techniques. Fig. 3 shows a schematic diagram of the experimental apparatus. The apparatus consisted of a rotating arm with a 632.8 nm Helium-Neon laser mounted at the far end. A fibre holder was secured on the rotating arm at its axis of rotation (165 mm from the laser) and was allowed to move 10 mm along the fibre axis. The fibre was placed in the grooves of the fibre holder and held tightly in place with super glue. This rotating arm was secured on a platform, which had 2.5° intervals marked on the platform from 0.0° to 90.0°. A second rotating arm contained a moveable observation screen (400 mm by 550 mm). This screen was kept perpendicular to the fibre axis and was allowed to move along the fibre axis. The screen consisted of a fine grain tracing paper. This was the best material available as it was fine enough to allow a clear image to be obtained on the screen, and it was translucent enough for the image to be photographed by rear-projection. The screen had an LED fixed at each corner. The four LED's were used as a frame of reference in the photographic image to locate the coordinates of the fibre axis and, hence, the centre of the observed image. A camera was fixed in position 1600 mm from the screen. With the rotating arm at 0.0°, that is an angle of incidence of 90.0°, the grooves of the fibre holder were used to align the fibre so that it was at 90.0° to the observation screen. At this point, a bright spot was observed on the screen. This bright spot was recorded by rear projection to provide a reference point for the centre of the image for subsequent images. The laser was then rotated to the required angle of incidence i, that is: $i = 90° - \gamma$, where γ is the beam-fibre angle. The observed image was then recorded and analysed using image analysis software. The initial image of the bright spot, without the fibre, was also used to determine the background noise of the image produced by the image process (photographing and processing), by taking the intensity profile along the line Y_oY_f away from the bright spot. It was necessary to carry out the experiment in a dark room with varying aperture settings and exposure times because the rings, or section of rings, were sometimes very faint. Furthermore, it was found that using small beam-fibre angles ($\gamma < 30°$) produced rings with greater intensity. This also accommodated the geometry of the apparatus.

In this study, both conventional and digital photographic techniques were used to record the images. For conventional photography a 35 mm camera with 400ASA black and white film (processed as 800ASA) was used. The negatives were then scanned using a Nikon LS2000 negative scanner, with $4\times$ multi-sample, wide gammet and 12 bit greyscale. For digital photography a JVC TK-F7300u frame capture digital camera was used and HRCAP software to drive the camera. The digital image size obtained in both cases was 736×576 pixels. Images of 2477×1681 pixels were also used but these images produced the same results as the smaller images.

The top left-hand corner of the image had the coordinates of (0, 0), while the bottom right-hand corner of the image had the coordinates of (735, 575) and (2476, 1680) for the larger images. Using image

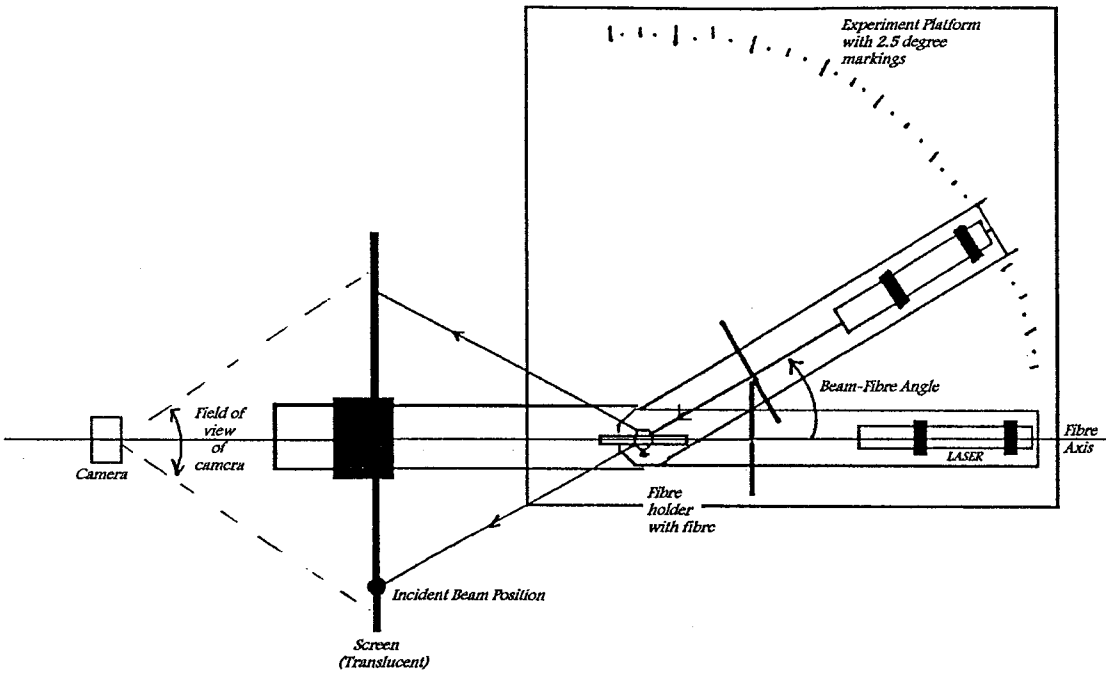

(a)

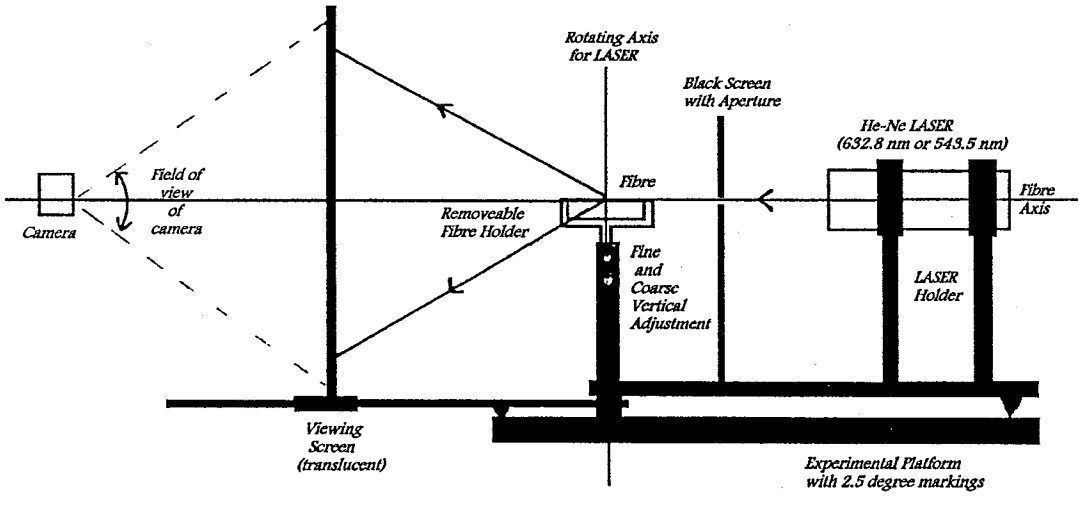

(b)

Figure 3 a and b show a top-view and side-view of the experiment set-up, respectively.

analysis software[1] and the frame of reference given by the position of the image produced by the four corners LED's, the coordinates of the incident beam position and the coordinates of the centre of the image were found. All measurements and intensity profiles were obtained relative to the centre of the image. Each pixel in the image was assigned a greyscale value between 0 and 255. It was not found necessary to convert the greyscale to intensity as this greyscale was adequate to locate the position of the rings.

A scaling factor for the image was needed to scale the measurements made from the image. This was achieved by photographing a ruler at the screen level, keeping all other distances unaltered. The dimensions of the frame of reference were also used to verify the scaling factor.

[1]The Imaging Processing Program used to obtain the intensity profiles was the UTHSCA Image Tool program developed at the University of Texas Health Science at San Antonio, Texas and available from the internet by anonymous FTP from ftp://maxrad6.uthsca.edu.

When all scaling factors were the same, the image was analysed.

3. Discussion and calculations

To understand the observed scattering pattern shown in Fig. 1, the simplest model of a long smooth cylindrical homogeneous reflecting fibre of circular cross-section, which can be easily explained by geometric optics and ray tracing techniques, will be considered. It will be assumed that the fibre has a radius a and is of a homogeneous, optically isotropic dielectric material. A perturbation, such as a taper, which can also be easily treated using ray-tracing techniques, will then be introduced to this cylindrical fibre.

Light of cross-sectional area of beam greater than the diameter of the fibre and incident obliquely on an infinitely long fibre will be partially reflected, partially transmitted and perhaps absorbed by the fibre. The effects of transmission of light through the fibre and the

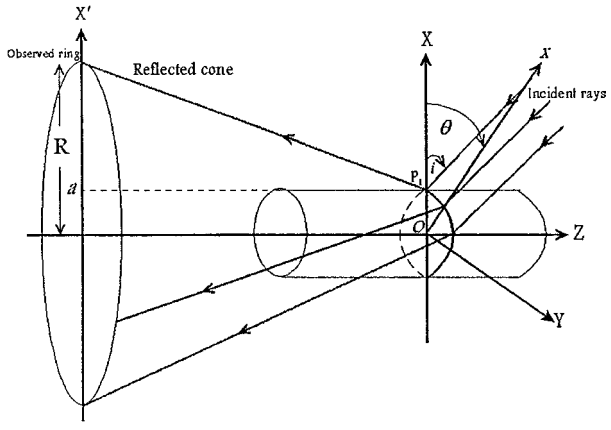

Figure 4 Geometry of reflection from a fibre for oblique incidence, where a is the radius of the fibre and R is the radius of the reflected ring formed in the observation plane.

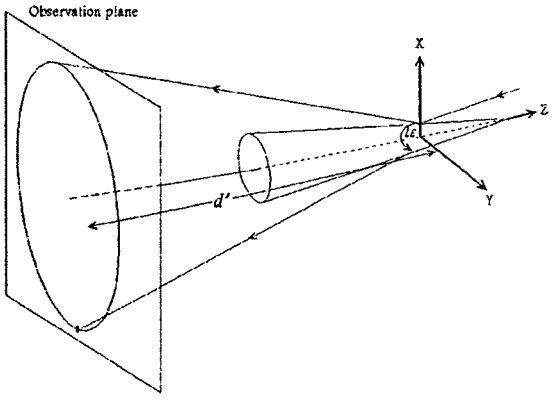

Figure 5 Section of a conical fibre showing co-ordinate system. The orientation of the fibre given above corresponds to the negative fibre orientation.

effects of refraction, internal reflections and scattering within the fibre can be eliminated by applying a very thin metallic (chromium or gold) coating on the fibre so that only reflection occurs. This enabled reflection from the the scale profile of the fibre to be observed. Although the incident and reflected light rays and surface normal lie in the same plane of incidence, they are not coplanar with the fibre axis but skew around it as the surface normal changes with the point of incidence on the fibre. The plane of incidence for each ray changes as the surface normal rotates around the fibre surface, as does the angle of incidence of the light ray.

The reflected light can be traced from the point of reflection to the point where it intersects the observation plane perpendicular to the fibre axis at some distance d from the fibre. To do so the incident light will be viewed as an infinitely large number of parallel rays, and the reflected ray will be specified by its direction cosines and the coordinates of the point at which it leaves the fibre surface in a right-handed Cartesian co-ordinate system (see Fig. 4).

In such a system, the incident rays all lie in the XZ plane. For a single incident ray which makes angles α, β, and γ with the OX, OY and OZ axes respectively, the direction cosines are defined by:

$$(\cos\alpha, \cos\beta, \cos\gamma) = (-\sin\gamma, 0, -\cos\gamma) \qquad (2)$$

where in the XZ-plane i is the angle of incidence. In this plane, $\alpha = \pi/2 - \gamma$ and $\beta = 0$. The point P_1 is also defined by:

$$P_1 = (a \cdot \sin\theta, a \cdot \cos\theta, 0) \qquad (3)$$

where a is the fibre radius and θ is the angle of the surface normal defined by the axis ox at P_1. The direction cosines of the reflected ray at P_1 are defined by:

$$(\cos 2\theta \cdot \cos i, \sin 2\theta \cos i, \sin i) \qquad (4)$$

The rays reflect in a cone thus forming circular rings at the observation plane, perpendicular to the fibre axis at some distance, d, from the point of incidence. The geometric path of the reflected light, ℓ is defined as

$$l = \left(d \cdot \frac{\cos 2\theta}{\tan i} + a\cos\theta\right)\hat{i} + \left(d \cdot \frac{\sin 2\theta}{\tan i} + a\sin\theta\right)\hat{j} - (d)\hat{k} \qquad (5)$$

The geometric path of each ray intersects the observation plane forming a circular ring whose radius is characterised by the observation distance and angle of incidence, i, shown in Fig. 4.

Natural fibres are not cylindrical, but deviate from the ideal circular cylinder of uniform cross-sectional area, due to their scale nature. Therefore, it is appropriate to introduce a small perturbation to the fibre, and since the scales are inclined at small angles to the fibre axis, the simplest perturbation to consider is a small taper in the fibre. The fibre is now viewed as a cone of circular cross-section, which subtends an angle of 2ε at the vertex, as shown in Fig. 5.

Following the same argument as before, for such a fibre light reflected from its surface at point P_1 is now defined by:

$$(\cos\alpha, \cos\beta, \cos\gamma) \qquad (6)$$

where

$$\begin{aligned}\cos\alpha &= (\cos^2\theta\cos 2\varepsilon - \sin^2\theta)\cos i \\ &\quad - \cos\theta\sin 2\varepsilon\sin i \\ \cos\beta &= \frac{1}{2}(\sin 2\theta(\cos 2\varepsilon + 1)\cos i + 1) \\ &\quad - \sin\theta\sin 2\varepsilon\sin i \\ \cos\gamma &= \cos\theta\sin 2\varepsilon\cos i + \cos 2\varepsilon\sin i\end{aligned} \qquad (7)$$

The geometric path for this reflected ray is defined by:

$$l = (X)\hat{i} + (Y)\hat{j} - (d)\hat{k} \qquad (8)$$

where

$$X = d\frac{(\cos^2\theta\cos i\cos 2\varepsilon - \sin^2\theta\cos i - \cos\theta\sin i\sin 2\varepsilon)}{\cos\theta\cos i\sin 2\varepsilon + \sin i\cos 2\varepsilon} \qquad (9a)$$

$$Y = d\frac{\left(\frac{1}{2}\sin 2\theta\cos i(\cos 2\varepsilon + 1) - \sin\theta\sin i\sin 2\varepsilon\right)}{\cos\theta\cos i\sin 2\varepsilon + \sin i\cos 2\varepsilon} \qquad (9b)$$

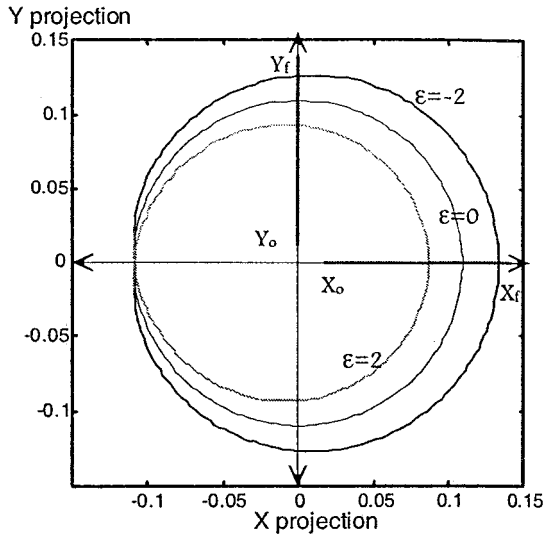

Figure 6 Projection of the reflected ray for light incident at an angle of 70° on a cone, which subtends an angle of 4° (i.e., 2ε) at the vertex for both fibre orientations. The centre ring corresponds to the projection of light reflected from a circular cylindrical fibre for the same angle of incidence. The line X_oX_f and Y_oY_f represent the line along which the intensity profiles were taken.

The geometric path of each ray now intersects the observation plane forming a ring, which deviates from the circle. The ring thus formed is characterised by the observation distance, angle of incidence and the angle the cone subtends at the vertex. Fig. 6 shows the rings obtained for 3 cone angles. The angle the cone subtends may be positive or negative, depending on whether the light is incident from the base of the cone or the apex of the cone, respectively. Fig. 7 illustrates both the negative and positive orientations.

If we now consider the fibre as consisting of a series of cones subtending a range of angles at their virtual vertices, as shown in Fig. 8, then light reflecting from each cone will form a ring and all of these rings will meet at one point as shown in Figs 6 and 8. The scattering pattern shown in Fig. 1 clearly shows such rings. The fibre that produced this image has a specific scale profile. Each scale on this profile can be considered as part of a cone. Furthermore, since the screen distance is very large compared to the length of fibre illuminated (which is 5.5 ± 0.5 mm at an angle of incidence of 70°), the cones subtending the same angle at their virtual vertices will reflect light into the same ring. This results in a number of prominent rings, as is evident in Fig. 1, indicating that even though some 300 scales are illuminated only a few dominant scale angles are present.

If the fibre is modelled as a series of cone sections then it is possible to determine the angle each cone subtends at its virtual vertex and hence the scale angle. This method of determining the scale angles has the advantage of giving not only the average but all possible scale angles illuminated.

The geometric path of light for the rings resulting from each conic section is given by Equations 8 and 9. The scale angle can be calculated by determining the coordinates of the rings where they intersect either the line X_oX_f or Y_oY_f. This is achieved by taking the intensity profile along the line X_oX_f or Y_oY_f, that is $Y = 0$ or $X = 0$ respectively (refer to Figs 2 and 6) and using the dimensionless ratio $X_\varepsilon/X_{\varepsilon=0}$ or $Y_\varepsilon/Y_{\varepsilon=0}$. The obvious approach for determining the scale angle is to use the intensity profile along X_oX_f and the ratio $X_\varepsilon/X_{\varepsilon=0}$, where X_ε and $X_{\varepsilon=0}$ are the X-coordinates of the rings, along the line X_oX_f, and

$$\frac{X_\varepsilon}{X_{\varepsilon=0}} = \frac{\tan i}{\tan(i+2\varepsilon)}$$

From Fig. 2 it is seen that not all of the rings which intersect the line X_oX_f converge at the point P, as the 'rings' in this area appear to be more complex, showing more structure. This approach was, therefore not used. The nature of this apparent complex structure will be explained elsewhere.

The rings which intersect the line Y_oY_f can easily be seen to converge at the point P, therefore this line is used in preference to the line X_oX_f. The dimensionless ratio $Y_\varepsilon/Y_{\varepsilon=0}$ is used where Y_ε and $Y_{\varepsilon=0}$ are the Y-coordinates of the rings, along the line Y_oY_f (refer to Fig. 6). The coordinate ratio $Y_\varepsilon/Y_{\varepsilon=0}$ is given by:

$$\frac{Y_\varepsilon}{Y_{\varepsilon=0}} = \frac{\sin 2\theta \cdot \sin 2i \cdot (\cos 2\varepsilon + 1) - 4\sin\theta \sin^2 i \cdot \sin 2\varepsilon}{2(2\cos\theta \cdot \cos^2 i \cdot \sin 2\varepsilon + \sin 2i \cdot 2\varepsilon)} \tag{10}$$

Also along the OY axis, $X = 0$ and Equation 9a reduces to:

$$\cos\theta = \frac{1}{2}\tan i \cdot \tan\varepsilon + \left[\left(\frac{1}{2}\tan i \cdot \tan\varepsilon\right)^2 + 2\cos^{-2}\varepsilon\right]^{\frac{1}{2}} \tag{11}$$

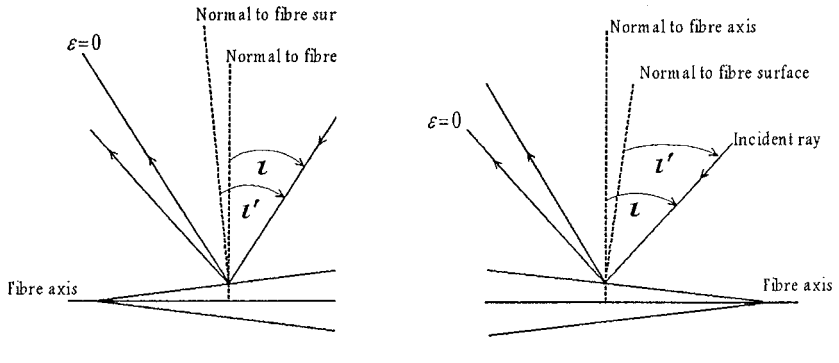

Figure 7 Illustrations of the negative and positive orientations of the fibre.

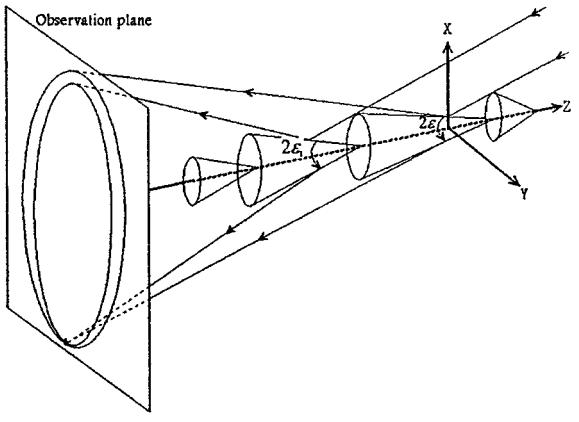

Figure 8 Fibre model: section of a conical fibre showing the orientation of the fibre with cones of varying angles subtended at the vertices (negative orientation).

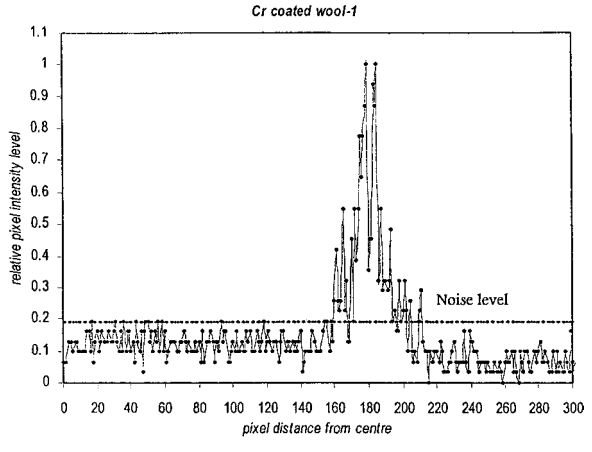

(a)

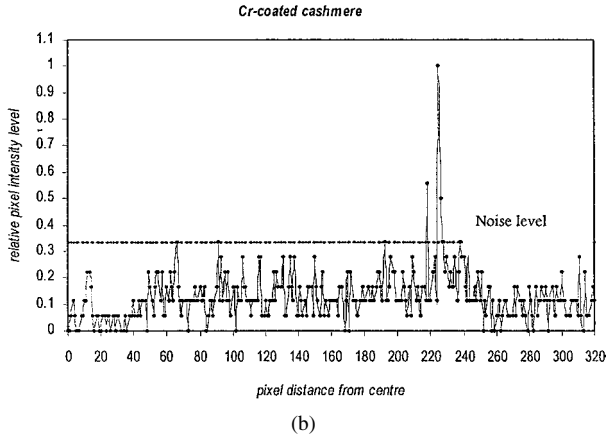

(b)

Figure 9 (a) The intensity profile of Cr-coated wool fibre, shown in Fig. 2. Only peaks above the noise level were considered in the scale-angle calculation. (b) The intensity profile of Cr-coated cashmere fibre. Only peaks above the noise level were considered in the scale-angle calculation.

From Equations 10 and 11 a curve of $\frac{Y_\varepsilon}{Y\varepsilon=0}(\varepsilon)$ was obtained. Using the curve of $\frac{Y_\varepsilon}{Y\varepsilon=0}$ against ε the scale angles for a given i were determined for all the coordinate ratios $Y_\varepsilon / Y_{\varepsilon=0}$ obtained from the intensity profiles.

Using the program Image Tool an intensity profile, as seen in Figs 9 and 10, was obtained along the line defined by $X = 0$ (the line $Y_\mathrm{o}Y_\mathrm{f}$ shown in Fig. 1). The major rings due to reflection from scales produced several distinctive peaks in this profile and from these peaks Y_ε was determined. The coordinate ratio, $Y_\varepsilon / Y_{\varepsilon=0}$

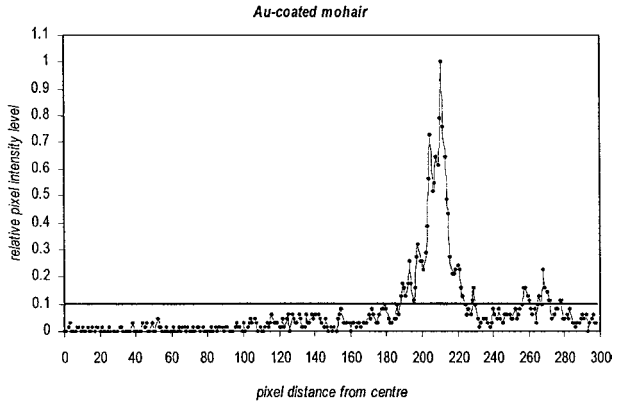

Figure 10 The intensity profile of Au-coated mohair fibre. Only peaks above the noise level were considered in the scale-angle calculation. In this figure, the relative pixel value is given as a function of pixel from centre.

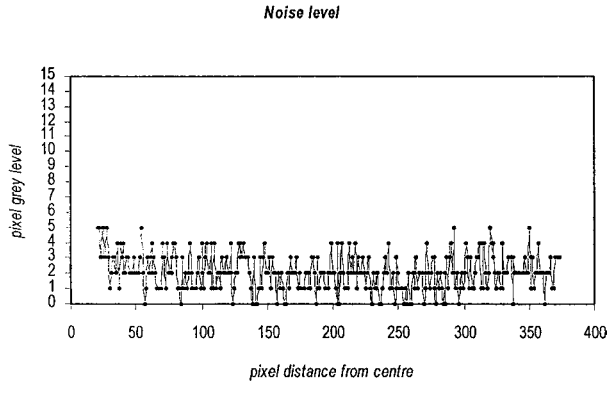

Figure 11 The noise level associated with images taken using the digital camera.

was then calculated for each peak and its corresponding scale angle interpolated from the curve of $\frac{Y_\varepsilon}{Y_{\varepsilon=0}}$ against ε. Only peaks above the noise level were considered. The noise level shown in Figs 9 and 10 was obtained using the image of the bright spot. The intensity profile for this noise level is shown in Fig. 11. The intensity profile for the chromium-coated wool fibre shown in Fig. 1 is given in Fig. 9a. Fig. 9b shows an intensity profile of a chromium-coated cashmere fibre.

Fig. 10 shows the intensity profile for a mohair fibre and the prominent scale angles corresponding to the main peaks are shown in Table I. The results obtained for three different chromium coated wool fibres are given in Tables II and III. These results were obtained from the intensity profiles taken with the digital

TABLE I Experimental values for scale angles for Au-coated mohair fibre, for light incident at an angle of 70° with wavelength of 632.8 nm and for the negative orientation of the fibre

$Y_{\varepsilon=0}$ (in pixels) ± 3 pixels	Y_ε (in pixels) ± 1 pixels	$\varepsilon^\circ \pm 0.05$	Relative peak heights
195	193	0.1	0.26
	198	−0.2	0.32
	200	−0.3	0.26
	205*	−0.6	0.73
	208	−0.8	0.65
	211*	−1.0	1.00
	215	−1.2	0.45
	220	−1.5	0.24
	268	−3.6	0.26

TABLE II Experimental values for scale angles for Cr coated wool fibres for light incident at an angle of 70° with wavelength of 632.8 nm and for the negative orientation of the fibre

Fibre	$Y_{\varepsilon=0}$ (in pixels) ± 3 pixels	Y_{ε} (in pixels) ± 1 pixels	$\varepsilon^{\circ} \pm 0.05$	Relative peak heights
Coarse wool fibre	183	279	−5.5	0.80
		261*	−4.6	1.0
		253*	−4.2	1.0
		249*	−4.0	1.0
		245	−3.8	0.80
		230	−3.0	0.80
		228*	−2.9	1.0
		221	−2.5	0.67
		216	−2.2	0.75
Fine wool fibre	183	244*	−3.8	1.0
		235*	−3.3	1.0
		230*	−3.0	1.0
		224	−2.6	0.89
		221*	−2.5	1.0
		216	−2.2	0.89
		231	−2.0	0.75
Super fine wool fibre	183	231	−3.0	0.67
		227	−2.8	0.83
		225*	−2.7	1.0
		222	−2.5	0.67
		216	−2.2	0.83

TABLE III Experimental values for scale angles for Cr coated wool fibres for light incident at an angle of 70° with wavelength of 632.8 nm and for the positive orientation of the fibre

Fibre	$Y_{\varepsilon=0}$ (in pixels) ± 3 pixels	Y_{ε} (in pixels) ± 1 pixels	$\varepsilon^{\circ} \pm 0.05$	Relative peak heights
Coarse wool fibre	240	125	8.6	0.89
		126	8.5	0.67
		144*	6.7	1.0
		184*	3.4	1.0
		229	0.6	0.89
		237	0.2	0.75
Fine wool fibre	240	135	7.6	0.67
		136	7.5	0.88
		168*	4.7	1.0
		208*	1.9	1.0
		228	0.7	0.88
		231	0.5	0.88
Super fine wool fibre	240	189	3.1	0.75
		191*	3.0	0.94
		192*	2.9	0.94
		193*	2.8	1.0
		194*	2.8	1.0
		196	2.6	0.80
		197	2.6	0.67

camera. The results show the distribution of scale angles of scales that were illuminated by the incident beam for three different wool fibres and for both positive and negative orientations. The maximum peaks of the intensity profile are marked with asterisks in the tables. These maximum peaks correspond to prominent rings in the scattering pattern, indicating that only a few prominent scales angles occur repeatedly within the illuminated section. The results show the range of scale angles for coarse wool, fine wool and super fine wool fibres to be: 0.2° to 8.6° ± 0.05°, 0.5° to 7.6° ± 0.05° and 2.2° to 3.0° ± 0.05°, respectively, Fourt [8] found the average scale angle for wool to be 3.7° with a range of 2.7° to 4.5°. The results obtained here are consistent with this average. The results also show that a greater range of scale angles exist for coarse wool fibre than for fine wool fibres.

Each pixel corresponds to an angle of 0.08° subtended at the image or observation plane. There was an uncertainty of ±3 pixels in locating the centre of the image. This corresponds to a possible ±3 pixel shift in every peak or an estimated ±0.3° in the absolute value of the scale angle. To determine the uncertainty in each scale angle, from Table II, $\delta(Y_{\varepsilon}) = 18$ pixels, which corresponds to $\delta(\varepsilon^{\circ}) = 0.9^{\circ}$. Therefore, if there is an uncertainty of 1 pixel in locating each peak, then the estimated uncertainty in the scale angle is ±0.05°. The scales marked with asterisks are the scale angles corresponding to the main peaks.

The results for several other fibres (wool, cashmere and mohair) are summarised in Tables IV–VII. These tables only show the ranges of scales for all fibres. These results show that with each fibre orientations both positive and negative scale angles corresponding to prominent intensity peaks are observed. This suggests that although most of the scales are inclined in the same direction each fibre has a few scales that are inclined in the opposite direction. Swift [9] refers to these 'opposite' scales as "false scales".

It is thought unlikely that these 'opposite' scales are due to complete scales but rather associated with these "false scales" caused by small scale fragments that chip away eliminating some of the cuticle. It is known that the scale pattern changes gradually one centimetre above the root as scale edges chip away to yield irregular contours [9]. The pattern of the scale edges, according to Swift, depends upon the cross-sectional shape of the fibre, that is, for fibres that have irregular cross-sections, "the scales wear away more rapidly in the regions of greatest overall convexity". This convexity is the result of the natural twist along the fibre and, therefore, the fibre crimp [9–11].

Measurements of scale angles were also made at different positions along the fibre. The results show that there is a variation in scale angles along the length of the fibre. This is shown in Tables VI and VII where the scale angle range for positions 1 to 5 of uncoated wool 1 show a variation, similarly for positions 1 to 3 of uncoated wool 2. Also, a small but apparent variation in the scale angle was observed at two positions around the circumference of the fibre, as shown for uncoated wool fibre 3 in Tables VI and VII. Thus, each scale angle observed appears to be associated with only part of the cone in the cone model adopted. The fibres can therefore be considered to consist of irregular and incomplete cones where each of these irregular and incomplete cones subtends an angle given by the scale angle at their virtual vertex. These irregular and incomplete cones may be attributed to the different thickness of the cuticle around the fibre due to the greater degree of overlap of the cuticle cells and, hence, the asymmetry of the fibre cross-sectional area [12, 13].

TABLE IV Experimental values from images obtained using digital camera for scale ranges for positive orientation of fibres. Wavelength used 632.8 nm

Fibre	$i \pm 3^\circ$	Scale angle range ($\pm 0.05^\circ$)	Negative scale angles recorded (if any) ($\pm 0.05^\circ$)
Cr coated wool no. 1	70°	5.7° to 0.3°	−0.4°, −0.7°, −1.1
Cr coated wool no. 2	70°	3.0° to 0.1°	None
Cr coated wool no. 3	70°	1.2° to 0.1°	None
Cr coated mohair no. 1	70°	0.9° to 0.1°	None
Cr coated cashmere no. 1	70°	1.0° and 0.2°	None
Au coated mohair no. 1	70°	1.0° to 0.3°	−0.5°
Au coated mohair no. 2	70°	1.3° to 0.3°	−0.5°
Au coated cashmere no. 1	70°	1.4° to 0.1°	−0.2°
Au coated cashmere no. 2	70°	2.2° to 0.3°	−0.3°
Au coated cashmere no. 3	70°	2.6° to 0.7°	−0.3°, −0.6°, −1.0°
Uncoated mohair	75°	0.5° to 0.1°	None
Uncoated cashmere	65°	0.7° to 0.4°	None

TABLE V Experimental values from images obtained using digital camera for scale ranges for negative orientation of fibres. Wavelength used 632.8 nm

Fibre	$i \pm 3^\circ$	Scale angle range ($\pm 0.05^\circ$)	Positive scale angles recorded (if any) ($\pm 0.05^\circ$)
Cr coated wool no. 1	70°	−2.1° to −0.4°	None
Cr coated wool no. 2	70°	−3.0° to −1.2°	None
Cr coated wool no. 3	70°	−1.1° to −0.6°	None
Cr coated mohair no. 1	70°	−0.9° to −0.1°	None
Cr coated cashmere no. 1	70°	−0.9° to −0.3°	None
Au coated mohair no. 1	70°	−1.0° to −0.1°	None
Au coated mohair no. 2	70°	−1.4° to −0.2°	0.2°, 0.4°, 0.5°
Au coated cashmere no. 1	70°	−1.2° to −0.4°	0.2°, 0.4°
Au coated cashmere no. 2	70°	−1.9° to −0.3°	0.4°
Au coated cashmere no. 3	70°	−2.0 to −0.3	None
Uncoated mohair	75°	−0.4° to −0.1°	None
Uncoated cashmere	65°	−0.7° to −0.1°	None

TABLE VI Experimental values from images obtained using conventional photographic method for scale ranges for positive orientation of fibres. Wavelength used 632.8 nm

Fibre	$i \pm 3^\circ$	Scale angle range ($\pm 0.05^\circ$)	Negative scale angles recorded (if any) ($\pm 0.05^\circ$)
Uncoated wool no. 1 position 1	70°	4.0° to 0.3°	−0.6°, −0.8°, −1.1°
Uncoated wool no. 1 position 2	70°	4.3° to 0.2°	−0.7°, −0.9°, −1.2°
Uncoated wool no. 1 position 3	70°	6.6° to 0.8°	None
Uncoated wool no. 1 position 4	70°	4.4° to 0.3°	None
Uncoated wool no. 1 position 5	70°	2.6° to 0.2°	−0.1°, −0.2°, −1.1
Uncoated wool no. 2 position 1	70°	2.1° to 0.5°	None
Uncoated wool no. 2 position 2	70°	2.5° to 0.3°	−0.5, −1.3
Uncoated wool no. 2 position 3	70°	2.3° to 0.2°	−0.2°, −0.3°, −1.3
Uncoated wool no. 3 position 1	70°	1.9° to 0.3°	None
Uncoated wool no. 3 position 1, rotated 150° about fibre axis	70°	2.7° to 0.4°	None
Au coated mohair no. 3	60°	1.0° to 0.9°	None
Au coated cashmere no. 4	60°	1.6° to 0.2°	−0.6°

TABLE VII Experimental values from images obtained using conventional photographic method for scale ranges for negative orientation of fibres. Wavelength used 632.8 nm

Fibre	$i \pm 3^\circ$	Scale angle range ($\pm 0.05^\circ$)	Positive scale angles recorded (if any) ($\pm 0.05^\circ$)
Uncoated wool no. 1 position 1	70°	−4.3° to −0.2°	0.3°, 0.4°, 0.6°, 1.1°
Uncoated wool no. 1 position 2	70°	−2.3° to −0.2°	None
Uncoated wool no. 1 position 3	70°	−4.9° to −0.4°	0.8°, 0.9°, 1.1°
Uncoated wool no. 1 position 4	70°	−4.1° to −0.2°	0.6°
Uncoated wool no. 1 position 5	70°	−2.6° to −0.3°	0.4°, 0.9°, 1.1°
Uncoated wool no. 2 position 1	70°	−2.2° to −0.2°	0.4°, 0.6°, 0.9°, 1.1°
Uncoated wool no. 2 position 2	70°	−3.3° to −0.4°	None
Uncoated wool no. 2 position 3	70°	−2.5° to −0.2°	0.3°, 0.5°, 0.7°
Uncoated wool no. 3 position 1	70°	−2.7° to −0.4°	None
Uncoated wool no. 3 position 1, rotated 150° about fibre axis	70°	−2.4° to −0.9°	None
Au coated mohair no. 3	60°	−1.0° to −0.9°	None
Au coated cashmere no. 4	60°	−1.2° to −0.4°	None

References

1. R. F. STAMM, M. L. GARCIA and J. J. FUCHS, *J. Soc. Cosmet. Chem.* **28** (1977) 571.
2. J. H. S. RENNIE, S. E. BEDFORD and J. D. HAGUE, *Int. J. Cosmt. Sci.* **19** (1997) 131.
3. N. J. J. VAN RESBURG and A. P. B. MAASDORP, in Proceedings of the 7th International Wool Textile Research Conference (1985) Vol. 1, p. 243.
4. Y. TANGO and K. SHIMMOTO, *J. Cosmt. Sci.* **52** (2001) 237.
5. A. GUIOLET, J. C. GARSON and J. L. LEVECQUE, *Int. J. Cosmt. Sci.* **9** (1987) 111.
6. H. K. BUSTARD and R. W. SMITH, *Int. J. Cosmet. Sci.* **12** (1990) 121.
7. C. RIECH and C. R. ROBBINS, *J. Soc. Cosmet. Chem.* **44** (1993) 221.
8. L. FOURT, *Textile Research Journal* **21** (1966) 899.
9. J. MENKART and R. J. BRAY, "Wool Handbook: A Text and Reference Book for the Entire Wool Industy," 3rd edn., edited by von Bergen (Intersciences, New York, 1970) p. 388.
10. M. HORIO and T. KONDO, *Textile Research Journal* **23**(6) (1953) 373.
11. B. P. BAXTER, *Wool Techn. and Sheep Breed.* **42**(2) (1994) 176.
12. K. R. MAKINSON, *Textile Research Journal*, October (1978) 598.
13. P. KASSENBECK, in Proceedings of the 1st International Congress on Hair Resaerch (Hamberg, March 13th–16th, 1979) p. 52.

Received 7 January
and accepted 7 July 2003